Proceedings of the ASME 2018
International Mechanical Engineering Congress and Exposition
IMECE2018
November 9-15, 2018, Pittsburgh, PA, USA

IMECE2018-86567

NUMERICAL INVESTIGATION OF INTERNAL FORCES DURING CARBON NANOTUBE FOREST SELF-ASSEMBLY

Taher Hajilounezhad
Mechanical & Aerospace Engineering
University of Missouri
Columbia, Missouri, USA

Matthew R. Maschmann
Mechanical & Aerospace Engineering
University of Missouri
Columbia, Missouri, USA

ABSTRACT

A time-resolved two-dimensional finite element simulation is developed to model the forces generated during the self-assembly of actively growing CNT populations with distributed properties and growth characteristics. CNTs are simulated as interconnected frame elements that undergo the base growth mechanism. Mechanical equilibrium at each computational node is determined at each time step using the Updated Lagrangian method. Emphasis is placed on the transmission of force to the growth substrate, where catalyst particles reside. The simulated CNT forest structural morphology is similar to that of physical CNT forests, and results indicate that stresses on the order of GPa are transmitted to catalyst particles. The force transmitted to a given catalyst particle is correlated to the rate at which the CNT grows relative to the population averaged growth rate. The effect of diameter-dependent CNT growth rates and the persistence of vdW bonds are also examined relative to the forces generated during forest self-assembly. Results from this study may be applied to the study of CNT forest self-assembly, resultant ensemble forest properties, and force-modulated CNT growth kinetics.

INTRODUCTION

Carbon nanotube (CNT) forests are populations of CNTs that self-assemble into vertically oriented films during their synthesis. CNT forests are typically synthesized using chemical vapor deposition (CVD) in which transition metal catalyst nanoparticles facilitate the conversion of gas-phase hydrocarbon species into solid CNTs. The catalyst particle may reside on the growth substrate during CNT growth (base growth), or it may reside at the tip of a growing CNT (tip growth). Using conventional CVD processes, CNT forest synthesis is generally observed to follow a base-growth mechanism, placing significance on catalyst-substrate interactions throughout the duration of CNT synthesis.

CNTs have numerous beneficial mechanical, thermal and electronic properties that make them desirable as advanced sensors [1, 2, 3], thermal interfaces [3-5], and electrical interfaces [6]; however, the engineering properties of CNT forests are often significantly diminished relative to properties of isolated CNTs. The attributes of individual CNTs within a forest, such as diameter, growth rate, stiffness, and areal density, are distributed, and functional relationships between these attributes and CNT forest morphology are not well understood. The distributed nature of these attributes creates strong heterogeneity within the forest, the physical effects of which remain poorly understood. Nevertheless, it is generally accepted that the wavy morphology of CNTs within forests have deleterious effects on ensemble properties, and efforts to understand and control forest morphology could lead to increased forest performance relative to mechanical, thermal, and electrical properties.

Mechanical interactions between growing CNTs in contact lead to crowding and a general vertical orientation of CNTs, normal to the growth substrate. When in close proximity, neighboring CNTs are attracted to each other and are held in contact by short-range van der Waals forces. The contacts provide mechanical resistance to free motion of CNTs. Because CNTs in contact may be growing at drastically different rates and may provide different effective stiffness in response to deformation, force is generated between contacting CNT pairs. The forces are transmitted through the CNT and are of sufficient magnitude to deform CNTs, leading to the typical tortuous CNT morphological appearance observed in experiments. The tortuous CNTs are intermixed with vertically oriented CNTs, suggesting mechanical competition during the growth process. Differences in interaction during growth can lead to drastically

different CNT alignment and tortuosity, even within the height of a single CNT forest. An example of relatively straight CNT morphology is compared to a more tortuous morphology in Fig. 1.

A lack of a detailed understanding governing the kinetics of growing and interacting CNTs hinders the ability of researchers to control the ensemble properties of CNT forests. The mechanical coupling among CNTs during forest growth undoubtedly plays an important role on CNT forest collective growth and self-assembly [9]. The complexity of the coupling is made more difficult by the distributed nature of CNT physical attributes. According to Puretzky et al. [8], CNT growth rates are non-linearly correlated to CNT diameter due the catalyst kinetics. Bedewy and Hart [9] utilized a two-CNT micro-mechanical unit cell to show that mechanical coupling among CNTs growing in contact may also present a significant limitation to the density and quality of CNTs in a forest. As numerous CNTs grow to form an increasingly more complicated and interactive network, the mechanical interactions within CNT forests become significantly more complex, and more resolved simulation techniques are required.

Here, we report a time-resolved mechanical finite element simulation of growing and interacting CNTs that readily facilitates the computation of distributed CNT forces as a function of CNT attributes. The length of individual CNTs is sub-divided into discrete and interconnected "frame" elements, with nodes positioned on the end points of the element. Each nodal point supports bending, axial load, and transverse load (3 mechanical degrees of freedom per node). CNT-CNT van der Waals interactions are simulated as truss elements that resist relative motion between CNTs in contact. The growth of CNTs is accomplished by adding new elements to the base of each CNT at discrete time steps, approximating the base-growth mechanism that is frequently observed for CNT forests. It is noteworthy to address that other CNT forest models assume CNTs act as isolated vertical beams [12,13], isotropic continua [14], bent and interacting beam segments [9], and unit cells of straight CNTs [15,16]; however, these models are exercised to estimate CNT forest mechanical performance and approximate CNT forest morphology information from post-synthesis observations. The current work investigates the time-resolved growth and self-assembly of CNT forests with an emphasis on how CNT physical attributes influence the mechanical forces and resultant CNT forest morphology.

EXPERIMENTAL DETAILS

A time-resolved finite element mechanical model was developed in MATLAB to support the simulation of a growing and interacting CNT population, as previously reported [7]. Each CNT is modeled as a series of interconnected elastic Euler-Bernoulli finite frame elements, each with six degrees of freedom corresponding to angular rotation, an axial displacement, and a transverse displacement at each of two nodes. Base growth is realized by adding one new beam element to the base of each CNT per discrete time step. CNT attributes such as inner and outer diameter, growth rates and orientation angle, etc. are assigned at the onset of the simulation and do not change once assigned. In this work, we have considered 200 uniformly spaced CNTs on a 20 μm substrate. The average orientation angle is 90°, normal to the growth substrate, with deviations from the average randomly assigned based on user defined standard deviation.

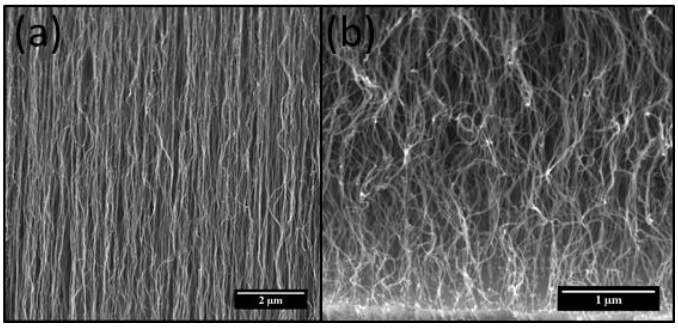

Figure 1. SEM micrographs of two different CNT forests that feature (a) a morphology that is well aligned and (b) a morphology that is highly tortuous and wavy in nature.

In the nucleation stage, the first row of finite elements are introduced, and physical attributes are assigned to each CNT individually. CNTs are uniformly spaced throughout the simulation domain, and the inner diameter of each CNT is assigned as 80% of the outer diameter. The outer diameters range from 5-15 nm and follow a Gaussian probability distribution. The orientation angle of the CNT relative to the growth substrate are similarly assigned to each CNT. Two types of growth rate distributions were studied in this work. One method randomly assigned growth rates to each CNT based on a Gaussian profile, while the other assigned growth rate based on the diameter-dependent relationship derived by Puretzky et al. [8]. The Young's modulus for all CNTs was 1 TPa, and each CNT was treated as a hollow cylinder with solid walls for the calculation of cross-sectional area and moment of inertia. Based on the length, area, orientation, modulus, moment of inertia of each element placed in the modeling domain, the stiffness matrix of the CNT forest system was computed. In the case of a 2D frame element, the stiffness matrix in local coordinates (aligned with the element axis), k, is stated as:

$$k = \begin{bmatrix} \frac{EA}{L} & 0 & 0 & \frac{-EA}{L} & 0 & 0 \\ 0 & \frac{12EI}{L^3} & \frac{6EI}{L^2} & 0 & \frac{-12EI}{L^3} & \frac{6EI}{L^2} \\ 0 & \frac{6EI}{L^2} & \frac{4EI}{L} & 0 & \frac{-6EI}{L^2} & \frac{2EI}{L} \\ \frac{-EA}{L} & 0 & 0 & \frac{EA}{L} & 0 & 0 \\ 0 & \frac{-12EI}{L^3} & \frac{-6EI}{L^2} & 0 & \frac{12EI}{L^3} & \frac{-6EI}{L^2} \\ 0 & \frac{6EI}{L^2} & \frac{2EI}{L} & 0 & \frac{-6EI}{L^2} & \frac{4EI}{L} \end{bmatrix} \quad [1]$$

where E is the elastic modulus, A is the cross sectional area, I is the second moment of inertia, and L is the length of the beam element. The local stiffness matrix is rotated into global coordinates and assembled into the global stiffness matrix using techniques described elsewhere [7].

The interactions between CNT elements within the domain are considered by assessing the distance between all nodal pairs in the system. Nodes with a distance of less than 50 nm are assumed to be in contact and are assigned a linear truss element to simulate van der Waals attraction. Note that this distance is the sum of the radius of each CNT and the separation between them. The truss elements are added to the CNT element stiffness matrices to form the global stiffness matrix. Entries into the global stiffness are rotated such that they share a common global coordinate system.

Growth of the CNTs within the forest is next considered. The bottom-most elements are stretched by 100% of their length along their axis. The displacement of all nodes in the system in response to the base growth (inclusive of the van der Waals contacts established between contacting CNTs) is found by solving the system of equations using the updated Lagrangian technique

$$\{R\}_t - \{F\}_{t-1} = [K]_t\{U\}_t \qquad [2]$$

where $\{F\}$ is a vector of internal forces, $\{R\}$ is a vector of applied forces to stretch the bottom-most elements, $[K]$ is the global tangent stiffness matrix, $\{U\}$ is the nodal displacement matrix, and the subscript t represents the current time step. After the nodal displacements are applied to the current nodal positions, the process starts again for a new time step.

RESULTS AND DISCUSSION

The current simulation offers significant flexibility towards studying the evolution of forces within growing CNT forests while providing robust quantitative characterization metrics. Individual parameters of interest may be isolated independently while keeping all other parameters constant. As an example, we consider the effect of the outer CNT diameter on CNT growth rate. If the bending stiffness of CNTs is the product of the Young's modulus (E) and the second area moment of inertia (I), then the bending stiffness of each CNT would scale as diameter to the forth power. Assuming that there is no functional relationship between CNT diameter and growth rate, then all CNTs are equally likely to experience tension or compression when contacting a neighboring CNT.

If, however, a direct relationship between CNT diameter and growth rate exists, then a significant non-zero force will be generated between two contacted CNTs of differing diameter. The large-diameter CNT will exhibit a relatively large bending stiffness and will also grow at a faster rate than the smaller-diameter CNT. Assuming the van der Waals contact between the CNTs is persistent, the larger-diameter and faster-growing CNT will produce a net tensile force on the smaller-diameter and slower-growing CNT in the pair. Further, the magnitude of the force generated will depend greatly on the diameter of the CNTs in contact because of the enhanced bending stiffness offered by large-diameter CNTs.

Alternatively, if van der Walls forces are not persistent and are allowed to break if a sufficient force is generated, then CNTs in contact may be relieved of excess strain when contacts are relinquished. In the following sections, the effect of diameter-dependent growth rates and the persistence of van der Waals forces are examined. The output metrics of interest include the force transmitted to the growth substrate (where the supporting catalyst particles reside) and the resultant morphology of the CNT forest.

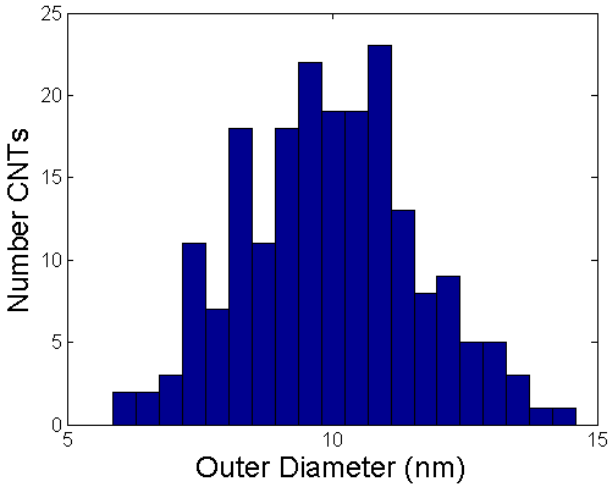

Figure 2. Histogram of CNT outer diameter for a simulated 200 CNT forest.

Effect of Diameter Variation on Growth Rate

In our previous works [7], we considered a constant diameter for all CNTs in a given forest for simulation simplification. In reality, CNT diameters are distributed in any CNT forest [10, 11]. Furthermore, reaction kinetics of CNT catalyst particles is diameter-dependent, suggesting that the growth rate of individual CNTs is related to their diameter. In light of these kinetics, we will employ a model developed by Puretzky that correlates maximum growth rate to CNT diameter [8]. Further, as Puretzky's model assumes CNT growth from a single carbon source, whereas there exist many hydrocarbons in a typical CVD process, a scaling factor is used to fit the quadratic function of outer diameter as [9],

$$\text{Growth Rate} = f(0.11d^2 - 0.02d + 0.36) \qquad [3]$$

where d is outer diameter of each CNT and f is a scaling function.

The current simulations considers a mean CNT outer diameter of 10 nm, as is commonly reported for CNT forests [18]. A Gaussian distribution of diameter of CNTs is assumed for simplicity, such that the minimum and maximum outer diameter of about 5 nm to 15 nm, respectively, was achieved.

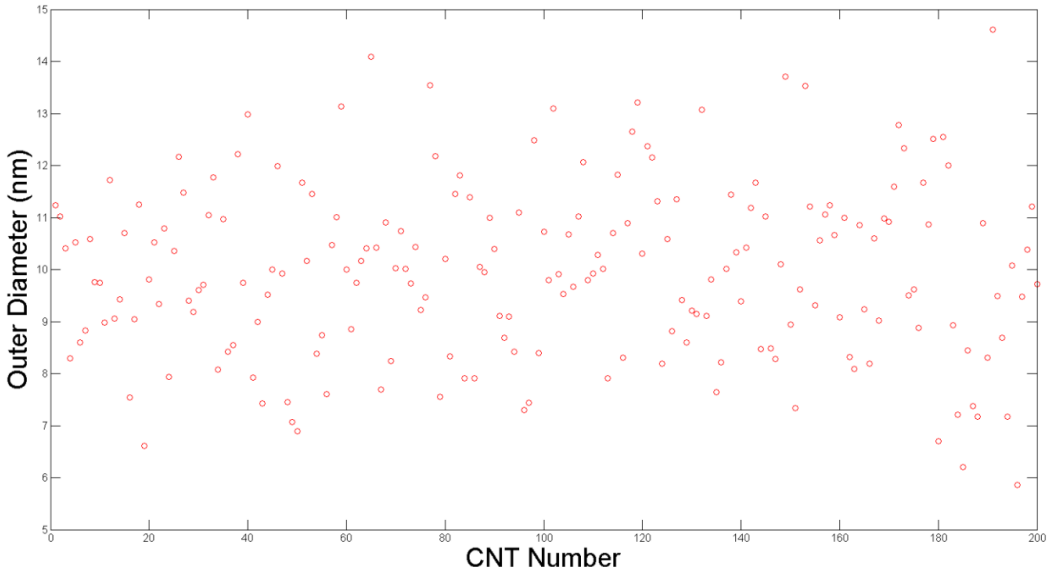

Figure 3. Distribution of CNT outer diameters within a 200 CNT forest corresponding to Figure 2.

Recall that CNT outer diameter was assigned randomly to each CNT in the simulation domain based on this Gaussian cumulative probability density function. The random assignment of CNT diameters is confirmed in Figure 3. A histogram of CNT outer diameter for a 200 CNT forest is shown in Figure 2. Note that the CNT diameters fall between 5 and 15 nm, as desired.

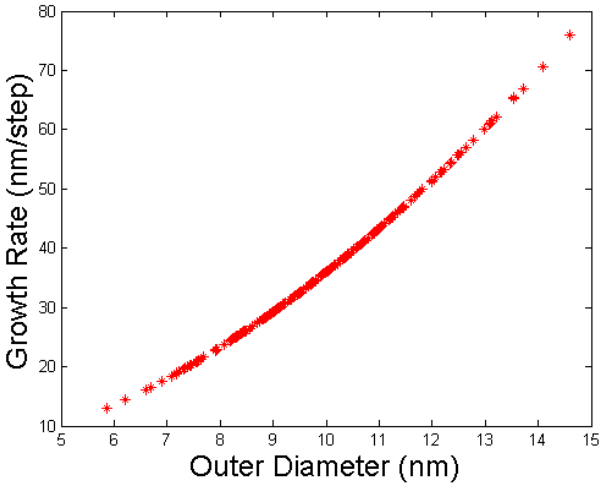

Figure 4. Growth rate as a function of CNT outer diameter corresponding to the CNT forest diameter histogram shown in Figure 2.

Practical limitations in simulation set the functional parameters for the growth rate relationship found in equation 3. In order to accurately capture CNT-CNT contact between adjacent CNTs, a maximum growth rate of 75 nm/time step was selected. If the length of CNT elements drastically exceeded this value, it may be possible for nodes of adjacent CNTs to not be detected for the sake of establishing van der Waals contacts.

Based on this upper limit, a mean growth rate of 36.6 nm/step was produced with a minimum growth rate of 12.91 nm/step. Note that the fastest growing CNT has a growth rate that is approximately 6x greater than that of the slowest growing CNT in the forest. A plot correlating the CNT growth rate as a function of outer diameter can be seen in Figure 4.

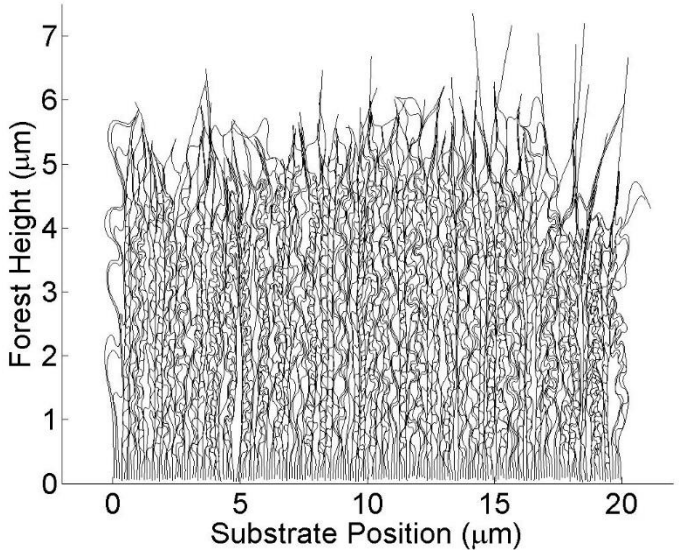

Figure 5. CNT morphology of a 200 CNT forest in which each CNT growth rate was determined by its outer diameter.

A simulation based on these inputs was allowed to run for a total of 200 time steps. In this simulation, the fastest growing CNTs grew for many time steps before contacting adjacent CNTs. This explains the top surface of the CNT forest, which has many non-interacting and straight CNTs extending from the main forest. The internal morphology of the CNT forest is quite tortuous, with many CNTs featuring a wavy profile. Note also

that embedded within the wavy morphology are many CNTs that are nearly vertical – seemingly pulled straight by interactions with neighboring CNTs. This morphology is quite similar to that CNT morphology obtained experimentally and shown in Figure 1b. The maximum height of the CNT forest is slightly greater than 7μm. When this height is divided by 200 (the number of simulated time steps), the average forest height advancement was 35 nm/step, in line with the population average growth rate of 36.6 nm/step.

The variable wavy and straight morphology of CNTs within the forest are consistent with the previous discussion that slower-growing CNTs would be pulled in tension, while faster-growing CNTs would bend when both were pinned in contact with each other. To further investigate this hypothesis, the axial force (defined in the local orientation of each CNT) transmitted to the base of each CNT was measured as a function of each time step from time steps 50-200. The first 50 time steps were omitted from the measurement because CNT-CNT contacts were not fully established during this time window. The forces generated by CNT-CNT interactions and transmitted back to the growth substrate is an important quantity because this force would interact directly with the catalyst particle itself. If mechanical sufficient stress is imparted to the catalyst, it may be possible to modulate CNT growth rates or even delaminate the CNT from the growth substrate.

Figure 6a shows the time-averaged axial force transmitted to the growth substrate as a function of CNT diameter. Forces range from almost 50 nN to -142 nN, with a clear nonlinear trend. Note that negative force corresponds to compression, while positive values correspond to tension. Because the CNT growth rate is related to outer diameter, the hypothesis that slower growing CNTs are being pulled in tension while faster growing CNTs are being restrained in compression is confirmed. In addition, loads change from tensile for diameters less than average diameter, i.e. 10 nm, to compressive for larger diameter CNTs. As growth rate is a function of diameter, similar behavior is displayed in Figure 6b where force is plotted versus growth rate rather than outer CNT diameter. While loading between individual CNTs has yet to be measured experimentally, previous CNT forest growth against a dead weight demonstrated that CNT forests grew against an average compressive force of 0.16 nN/CNT. It is not unreasonable to suggest that forces between individual CNTs may be orders of magnitude greater.

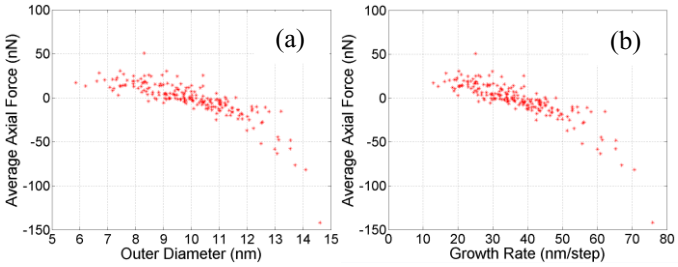

Figure 6. The time-averaged axial force exerted by each CNT at the growth substrate as a function of CNT outer diameter (a) sorted by outer diameter (b) versus growth rate variation.

Figure 7a depicts time-averaged axial stresses (defined as axial force divided by CNT cross-sectional area) transmitted to catalyst nanoparticles as a function of CNT outer diameter. Stresses in the range of about -2.35 GPa to 2.6 GPa are experienced by the CNT elements residing at the substrate. Assuming the base growth method, this stress is transmitted directly to the catalyst particle and may be of sufficient magnitude to modulate catalytic activity. It is remarkable that although axial force exhibit a non-linear trend with diameter, the stress varies almost linearly as a function of diameter and growth rate. Again, axial stress is plotted versus growth rate in Fig. 7b, and a nearly linear trend is once again presented.

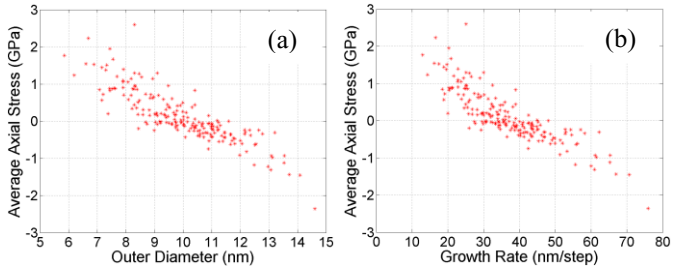

Figure 7. The time-averaged axial stress exerted by each CNT at the growth substrate as a function of CNT outer diameter (a) sorted by outer diameter (b) versus growth rate variation.

To examine the role of the diameter-dependent growth rate model, another simulation was run employing a different growth rate distribution. Here, the same discrete growth rates used in Figure 4 were utilized, but each was distributed randomly about the forest, independent of CNT diameter, as shown in Figure 8. In this simulation, all other parameters were identical to those used previously.

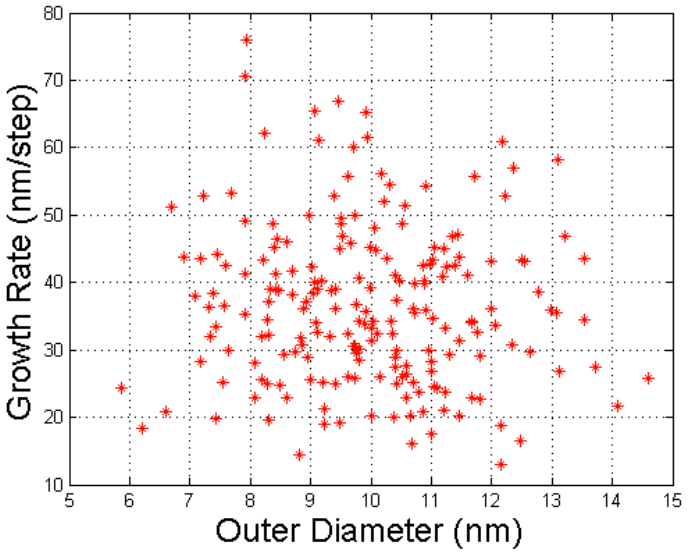

Figure 8. Growth rate distribution based on the random distribution of values of Figure 4.

Figure 9 shows that the CNT forest morphology of the diameter-independent CNT forest is quite similar to that produced when considering diameter-dependent growth rates. The top surface of the CNT forest is quite similar to the irregular surface produced by diameter-dependent growth rates. A mix of straight and wavy CNTs is again observed.

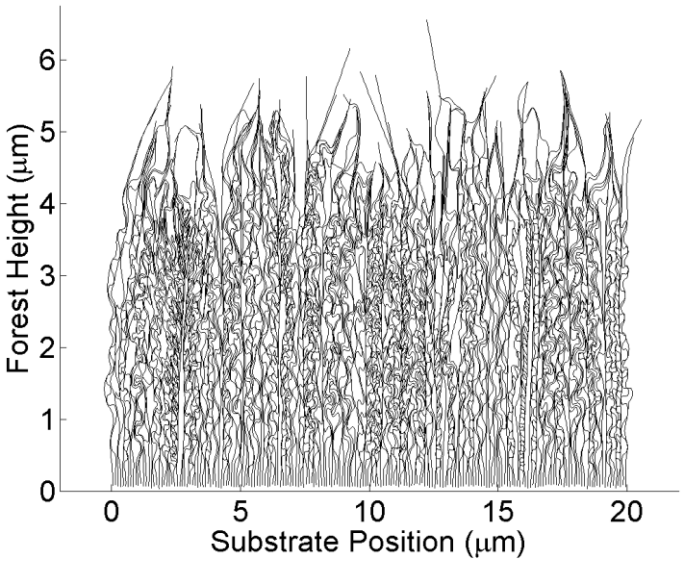

Figure 9. CNT morphology of a 200 CNT forest in which each CNT's growth rate was determined based on the random distribution of values of Figure 4.

The average axial force as a function of outer CNT diameter, shown in Figure 10a, shows that the magnitude of forces generated are similar to those generated with the diameter-dependent growth rates. Because the growth rates were distributed randomly, no correlation between axial force and diameter is seen. Figure 10b shows axial force versus growth rates. Again, relatively large positive force is transmitted to the slowest growing CNTs, corresponding to tension. Compressive forces are experienced by the fastest growing CNTs, while CNTs growing near the population average experienced neutral load on average.

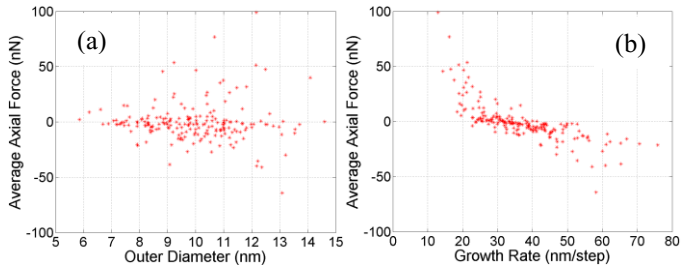

Figure 10. The time-averaged axial force exerted by each CNT at the growth substrate based on random distribution of growth rates (a) sorted by outer diameter and (b) versus growth rate.

Figure 11 depicts axial stresses transmitted to catalyst nanoparticles for the case of diameter-independent growth rates according to average axial force distribution shown in Fig. 10. Stresses in the range of about -1.65 GPa to 2.39 MPa are observed. Stresses are similar to those computed for the diameter-dependent growth rate, despite the random assignment of growth rate and diameter. No relationship exists between forces/stresses and diameter, as expected.

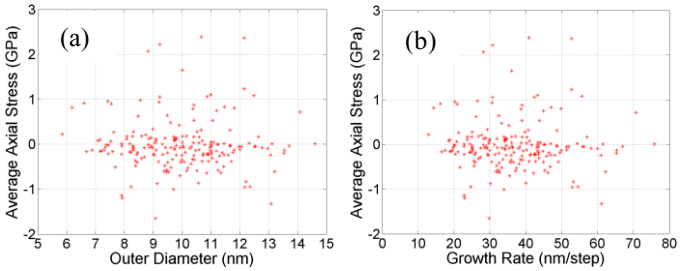

Figure 11. The time-averaged axial stress exerted by each CNT at the growth substrate based on random distribution of growth rates (a) sorted by outer diameter (b) versus growth rate.

Effect of van der Waals Bonds

As discussed earlier, when CNTs establish contact with neighbors, van der Waals forces act to hold contacting CNTs together. Collectively growing CNT pairs are subject to deformation and mechanical loading. Although the van der Waals bonds have been observed to persist in compressed CNT forests [20], they are not permanent and may break if tensile forces exceed a maximum value. If two CNTs in contact may be treated as parallel hollow cylinders, the force per unit length of contact is calculated as [17]

$$\frac{-A}{8\sqrt{2}D^{\frac{5}{2}}}\left(\frac{R_1R_2}{R_1+R_2}\right)^{1/2} \qquad [4]$$

where A is Hamaker constant, D is distance between outer diameters of two adjacent CNTs, and R_1 and R_2 are outer radii of neighboring nanotubes. To obtain an order of magnitude for this value, average values of CNT radius and length were analyzed, and the separation distance between contacting CNTs was assumed to be the interatomic layer spacing of graphite sheets, 0.34 nm. Also note that the value of the Hamaker constant was assumed to be 5×10^{-20}J [17]. For such a scenario, the average force required to break the van der Waals bond is 5 nN. Based on this representative value, van der Waals bonds experiencing a tensile force that exceeded this value were removed from the simulation, and liberated nodes were free to interact in the absence of the bond.

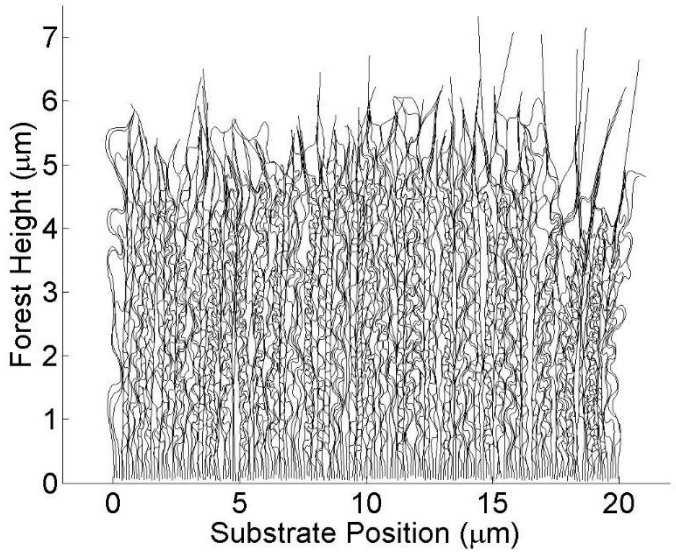

Figure 12. CNT morphology of a 200 CNT forest allowing vdW bond breakage.

Introducing this condition to van der Waals contacts had minimal influence on the CNT morphology, as shown in Figure 12. The CNT forest displayed represents the identical simulation conditions used to generate the CNT forest shown in Figure 5 with the addition of the conditional van der Waals bond. Only subtle differences between the two CNT morphologies may be observed. Obviously, the morphology dissimilarity and achieved heights would be more diverse if the simulation had been run for more time steps.

To better understand the subtle changes of the CNT morphology, the quantity of broken van der Waals contacts was evaluated at the end of each time step. Note that the number of nodes introduced during each time step is 200 corresponding to one additional node per CNT. One would also anticipate that the number of CNT-CNT bonds would also increase as a function of time as new nodes are introduced the system and deformation within the forest increases. As shown in Figure 13, no bonds were broken during the first 20 time steps. During this time the CNTs had not yet established neighboring contacts. As the length of CNTs and the number of CNT-CNT contacts increases. The number of broken CNT-CNT bonds also increases. In fact, the number of broken bonds increases nearly linearly until approximately 80 time steps, when the number of broken CNT-CNT bonds plateaus at about 2,000 / time step. The nature of this trend is under investigation; however, we believe that the distribution of CNT-CNT forces is greatest near the substrate. It is here that CNTs exhibit the greatest force to resist bending (proportional to $1/L^3$). These forces relax as CNTs grow longer, such that CNT-CNT bonds located sufficiently far from the growth substrate have less force acting on them and a lower probability of breaking.

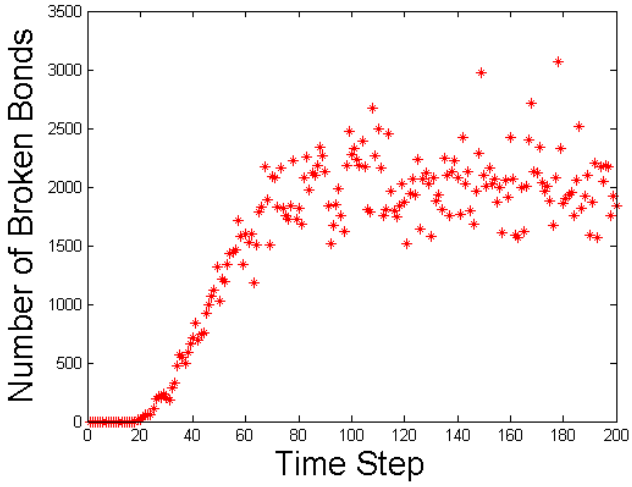

Figure 13. The number of broken bonds per time step due to excessive tensile forces.

Figure 14 exhibits the time-averaged axial force transmitted to the growth substrate as a function of CNT diameter when van der Waals bonds were allowed to break. Surprisingly, axial forces range from almost 60 nN to -155 nN – an increase in magnitude of approximately 10% when compared to persistent CNT-CNT contacts displayed in Figure 6. This trend is counterintuitive, as CNT-CNT pairs generating the most force are permitted to break in the latter case. However, in light of the cooperative nature of CNT forest networks, the force distribution within forests is complex. More research is being conducted to understand this phenomenon. We note that the transition between tensile and compressive forces occurs near the average outer diameter of 10 nm, as previously observed.

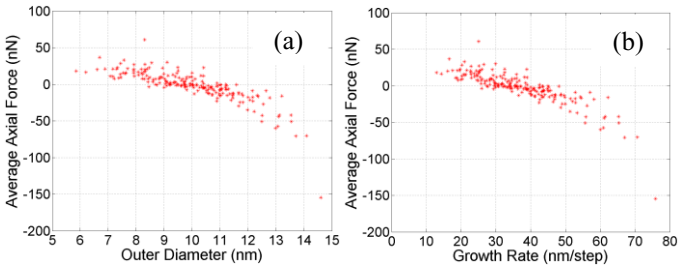

Figure 14. The time-averaged axial force exerted by each CNT at the growth substrate as a function of CNT outer diameter allowing vdW bonds breakage (a) sorted by outer diameter (b) versus growth rate variation.

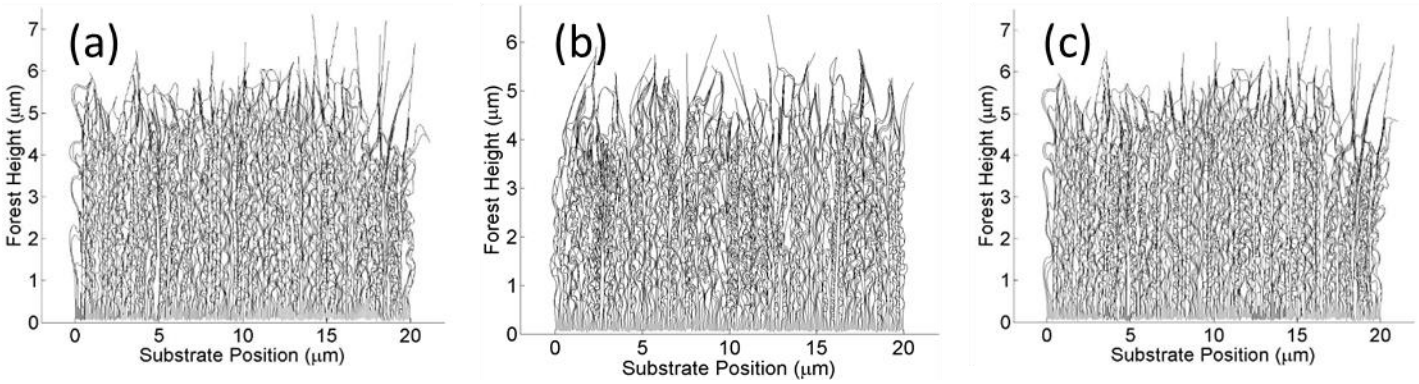

Figure 15. CNT morphology of a 200 CNT forest having (a) diameter-dependent growth rates, (b) randomly distributed growth rates, and (c) diameter-dependent growth rates while allowing vdW bond breakage.

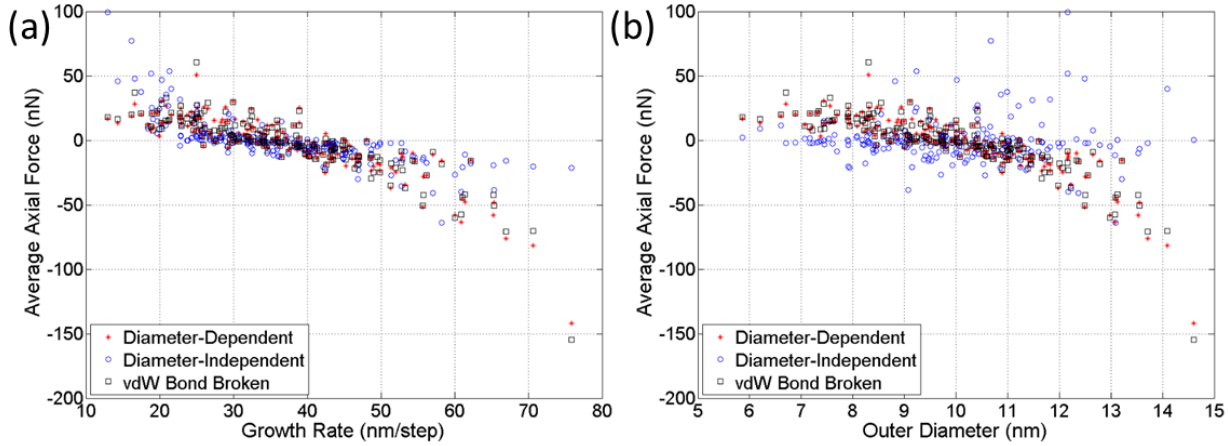

Figure 16. The time-averaged axial force exerted by each CNT at the growth substrate as a function of (a) CNT growth rate and (b)CNT outer diameter

Summary

For a ready comparison among various simulations, CNT forest morphologies are displayed consecutively in Figure 15. All forests feature similar input parameters and run for 200 time steps with 200 carbon nanotubes per forest. The largest morphology variation is attributed to the diameter-dependent growth rates. The effect of breaking vdW forces due to excessive tensile forces is shown in Figure 15c, with results most similar to the same forest growth with persistent vdW bonds (Figure 15a). This result suggests that broken vdW bonds may re-establish with neighboring CNTs in a manner similar to a case with persistent vdW bonds.

The time-averaged force transmitted to the substrate for these same cases is shown in Figure 16 as a function of diameter and growth rate independently. Note that in all cases, a negative correlation between growth rate and axial force at the substrate is evident (Figure 16a). Slowly growing CNTs are pulled in tension, while rapidly growing CNTs supply compressive force at the substrate. The diameter-independent growth rates generated the greatest tensile forces. Cross-referencing with Figure 16b shows that slow-growing CNTs with large tensile forces had diameters greater than the population mean of 10 nm. This scenario is not possible with diameter-dependent growth rates, whereby slow growing CNTs have small diameters. Interestingly, the average force experienced when introducing vdW bond breaking minimally alters the axial force, as one may intuitively predict that broken bonds would manifest in reduced forces within the forest.

CONCLUSIONS

CNT forest growth was simulated using a time-resolved finite element numerical model. Growth rates were applied randomly or from a mathematical model proposed by Puretzky et al. The CNT diameters were randomly assigned within the simulation domain. Results show that a strong correlation between axial force and CNT growth rate exists for all cases,

while a similar correlation between axial force and outer diameter exists when the growth rate is directly related to diameter. CNTs growing at a rate less than the population average exhibit a tensile force that increases in magnitude as growth rate decreases. Alternatively, CNTs growing at a rate that exceeds the population average exhibit a compressive force that increases in magnitude with increasing growth rate. Surprisingly, the existence of persistence van der Waals contact had little influence over CNT forest morphology when compared to van der Waals contacts that break at a tensile load exceeding 5 nN. These results are expected to contribute towards the understanding of CNT forest self-assembly and towards engineering CNT forests with desired ensemble properties.

ACKNOWLEDGMENTS

The authors would like to acknowledge funding from National Science Foundation (NSF) under award CMMI 1651538.

REFERENCES

[1] Yamada, T., Hayamizu, Y., Yamamoto, Y., Yomogida, Y., Izadi-Najafabadi, A., Futaba, D. N., and Hata, K., 2011, "A stretchable carbon nanotube strain sensor for human-motion detection," Nat Nano, 6(5), pp. 296-301.

[2] Maschmann, M. R., Ehlert, G. J., Dickinson, B. T., Phillips, D. M., Ray, C. W., Reich, G. W., and Baur, J. W., 2014, "Bioinspired Carbon Nanotube Fuzzy Fiber Hair Sensor for AirFlow Detection," Advanced Materials, 26(20), pp. 3230-3234.

[3] Cola, B., Xu, J., Cheng, C., Xu, X., Fisher, T., and Hu, H., 2007, "Photoacoustic characterization of carbon nanotube array thermal interfaces," Journal of Applied Physics, 101(5), p. 054313.

[4] Cola, B., Xu, X., and Fisher, T., 2007, "Increased real contact in thermal interfaces: A carbon nanotube/foil material," Applied Physics Letters, 90(9), p. 093513.

[5] Xu, J., and Fisher, T. S., 2006, "Enhancement of thermal interface materials with carbon nanotube arrays," International Journal of Heat and Mass Transfer, 49(9–10), pp. 1658-1666.

[6] Park, M., Cola, B. A., Siegmund, T., Xu, J., Maschmann, M. R., Fisher, T. S., and Kim, H., 2006, "Effects of a carbon nanotube layer on electrical contact resistance between copper substrates," Nanotechnology, 17(9), pp. 2294-2303.

[7] Maschmann, M. R., 2015, "Integrated simulation of active carbon nanotube forest growth and mechanical compression," Carbon, 86(0), pp. 26-37.

[8] A. A. Puretzky, D. B. Geohegan, S. Jesse, I. N. Ivanov and G. Eres, 2005, "In situ measurements and modeling of carbon nanotube array growth kinetics during chemical vapor deposition, "Appl. Phys. A, 81(0), pp. 223‐240.

[9] Bedewy, M., and Hart, A. J., 2013, "Mechanical coupling limits the density and quality of self-organized carbon nanotube growth," Nanoscale, 5(7), pp. 2928-2937.

[10] M. Bedewy, E. R. Meshot, M. J. Reinker and A. J. Hart, 2011, "Population Growth Dynamics of Carbon Nanotubes," ACS Nano, 5(11), pp. 8974‐8989.

[11] E. R. Meshot, D. L. Plata, S. Tawfick, Y. Y. Zhang, E. A. Verploegen and A. J. Hart, 2009, "Engineering Vertically Aligned Carbon Nanotube Growth by Decoupled Thermal Treatment of Precursor and Catalyst," ACS Nano, 3(9), pp. 2477‐2486.

[12] Maschmann, M.R., Zhang, Q., Wheeler, R., Du, F., Dai, L., and Baur J., 2011 , "In situ SEM observation of column-like and foam-like CNT array nanoindentation," ACS Appl Mater Interface, 3(3), pp.648–653.

[13] Cao, A., Dickrell, P.L., Sawyer, W.G., Ghasemi-Nejhad, M.N., and Ajayan, P.M., 2005, "Super-compressible foam like carbon nanotube films," Science, 310(5752), pp. 1307–1313.

[14] Hutchens, S.B., Needleman, A., and Greer, JR., 2011, "Analysis of uniaxial compression of vertically aligned carbon nanotubes," J Mech Phys Solids, 59(10), pp. 2227–2237.

[15] Gao, Y., Kodama, T., Won, Y., Dogbe, S., Pan, L., and Goodson, K.E., 2012, "Impact of nanotube density and alignment on the elastic modulus near the top and base surfaces of aligned multi-walled carbon nanotube films," Carbon, 50(10), pp.3789–3798.

[16] Won, Y., Gao, Y., Panzer, M.A., Xiang, R., Maruyama, S., and Kenny, T.W., et al., 2013, "Zipping, entanglement, and the elastic modulus of aligned single-walled carbon nanotube films," Proc Natl Acad Sci., 110(51), pp. 20426–20430.

[17] Israelachvili, J. N., 2011, Intermolecular and Surface Forces-3rd ed, Academic Press, Burlington, MA.

[18] Bedewy, M., Meshot, E. R., Guo, H., Verploegen, E. A., Lu, W. and Hart, A. J., 2009, "Collective Mechanism for the Evolution and Self-Termination of Vertically Aligned Carbon Nanotube Growth," J of Phys Chem C, 113(48), pp. 20576-20582.

[19] Maschmann, M. R., Dickinson, B., Ehlert, G. J., and Baur, J. W., 2012, "Force sensitive carbon nanotube arrays for biologically inspired airflow sensing," Smart Materials and Structures, 21(9), p. 094024.

[20] Maschmann, M. R. ., Ehlert, G. J., Park, S. J., Mollenhauer, D., Maruyama, B., Hart, A. J., and Baur, J. W., 2012, "Visualizing strain evolution and coordinated buckling within CNT arrays by in situ digital image correlation," Adv. Functional Materials 22 (22), pp. 4686-4695